Antiferromagnetic Mott insulating state in the single-component molecular material $Pd(tmdt)_2$

Rina Takagi,[1,*] Dita Puspita Sari,[2,3,4] Saidah Sakinah Mohd-Tajudin,[2,5] Retno Ashi,[2,3,4] Isao Watanabe,[2,3,5,6] Shoji Ishibashi,[7] Kazuya Miyagawa,[1] Satomi Ogura,[8] Biao Zhou,[8] Akiko Kobayashi,[8] and Kazushi Kanoda[1]

[1]*Department of Applied Physics, University of Tokyo, Bunkyo-ku, Tokyo 113-8656, Japan*

[2]*Advanced Meson Science Laboratory, RIKEN Nishina Center, Wako, Saitama 351-0198, Japan*

[3]*Department of Physics, Graduate School of Science, Osaka University, Toyonaka, Osaka 560-0043, Japan*

[4]*Department of Physics, Faculty of Natural Science, Institut Teknologi Sepuluh Nopember, Surabaya 60111, Indonesia*

[5]*Computational Chemistry and Physics Laboratory, School of Distance Education, Universiti Sains Malaysia, Penang 11800, Malaysia*

[6]*Muon Spin Resonance Laboratory, Department of Condensed Matter Physics, Faculty of Science, Hokkaido University, Sapporo 060-0810, Japan*

[7]*Research Center for Computational Design of Advanced Functional Materials (CD-FMat), National Institute of Advanced Industrial Science and Technology (AIST), Tsukuba, Ibaraki 305-8568, Japan*

[8]*Department of Chemistry, College of Humanities and Sciences, Nihon University, Setagaya-ku, Tokyo 156-8550, Japan*

(Received 18 October 2017; revised manuscript received 12 December 2017; published 26 December 2017)

A family of compounds built by a single molecular species, $M(tmdt)_2$, with a metal ion, M, and organic ligands, tmdt, affords diverse electronic phases due to M-dependent interplays between d electrons in M, and π electrons in tmdt. We investigated the spin state in $Pd(tmdt)_2$, a π-electron system without a d-electron contribution, through ^{1}H nuclear magnetic resonance (NMR) and muon-spin resonance experiments. The temperature profiles of the NMR linewidth, relaxation rate, and asymmetry parameter in muon decay show an inhomogeneous antiferromagnetic order with moments distributed around $\sim 0.1\mu_B$ that onsets at above 100 K. This result provides an example of the antiferromagnetic order in a pure π-electron system in $M(tmdt)_2$, and it demonstrates that correlation among the π electrons is so strong as to give the Néel temperature over 100 K. The small and inhomogeneous moments are understandable as the crucial disorder effect in correlated electrons situated near the Mott transition.

DOI: 10.1103/PhysRevB.96.214432

I. INTRODUCTION

The physics of strongly correlated electrons is one of the central issues in condensed-matter science. The notion of a Mott insulating state, in which correlation among electrons makes them localized, is considered a key concept for understanding various emergent phenomena such as metal-insulator transitions, unconventional superconductivity, and a variety of magnetism. Finding new Mott systems, especially residing close to the Mott transition, is expected to boost the search for novel phenomena and properties. A class of materials at the forefront of Mott physics is the family of molecular materials $M(tmdt)_2$ [1–3], which have recently been found to host highly correlated electrons [4–6] (tmdt is an abbreviation of trimethylenetetrathiafulvalenedithiolate).

The $M(tmdt)_2$ is a new type of molecular system composed solely of a single molecular species in which a transition-metal ion M is coordinated by molecular ligands, tmdt, from both sides [1–3], as shown in Figs. 1(a)–1(c). The molecular orbitals lying near the Fermi level, ϵ_F, are the $p\pi$ orbitals extended over the tmdt ligand and the $dp\sigma$ orbital located around M [7]. The energy-level difference between the $p\pi$ and $dp\sigma$ orbitals is varied by replacing M. For M = Ni, Pd, and Pt, the $dp\sigma$ orbitals are of higher energy than the $p\pi$ orbitals, which reside around ϵ_F and form conduction bands [1,8–10]. The two degenerate $p\pi$ orbitals accommodate two electrons, and thus the electronic bands are half-filled [1,4,9]. The M = Ni and Pt compounds are paramagnetic metals with appreciable electron correlation [4]. For the Ni compound, the de Haas–van Alphen oscillations pointed to semimetallic Fermi surfaces, which are consistent with the first-principles calculations [8,11]. Despite the similar crystal structure and electronic band structure, the Pd compound is semiconducting in resistivity [10]. The signal intensity of the electron paramagnetic resonance exhibits a sudden decrease below 100 K, and the ^{1}H nuclear magnetic resonance (NMR) spectrum becomes broadened at similar temperatures, pointing to an antiferromagnetic ordering [10]. Since the semimetallic Fermi surfaces predicted by the first-principles calculation have a form unsuitable for nesting, it is suggested that the magnetic ordering in $Pd(tmdt)_2$ is driven primarily by the electron correlation [10].

In the present study, we have made an in-depth characterization of the magnetic state in $Pd(tmdt)_2$ by detailed ^{1}H-NMR and muon-spin resonance (μSR) experiments. The antiferromagnetic ordering with inhomogeneity was unambiguously proved by the observation of NMR spectral broadening and muon-spin rotations, which demonstrates that the $p\pi$ electrons in $M(tmdt)_2$ can give an antiferromagnet with the Néel temperature exceeding 100 K. The moments are found to be distributed around the order of $0.1\mu_B$, which is argued in light of the disorder effect on the verge of the Mott transition.

II. EXPERIMENT

^{1}H-NMR and μSR experiments were carried out for an assembly of fine polycrystals of $Pd(tmdt)_2$. ^{1}H-NMR spectra and the nuclear spin-lattice relaxation rate, T_1^{-1}, were

[*]Present address: RIKEN Center for Emergent Matter Science (CEMS), Wako, Saitama 351-0198, Japan.

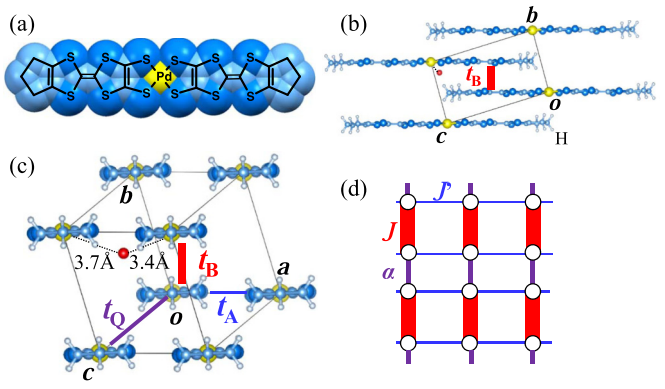

FIG. 1. (a) Molecular structure of $Pd(tmdt)_2$. (b),(c) Molecular arrangements in the $Pd(tmdt)_2$ crystal viewed along (b) the molecular short axis and (c) the molecular long axis. In (b) and (c), red spheres represent the center of muon distribution determined by an electrostatic potential calculation. The dotted lines are the closest contacts between the muon center and $Pd(tmdt)_2$ molecules. Transfer integrals for the bonds between the tmdt ligands along A: [100], B: [111], and Q: [001] are indicated as t_A, t_B, and t_Q, respectively. (d) Spin model for the $p\pi$ electrons localized on the tmdt ligands deduced from the transfer network in (c).

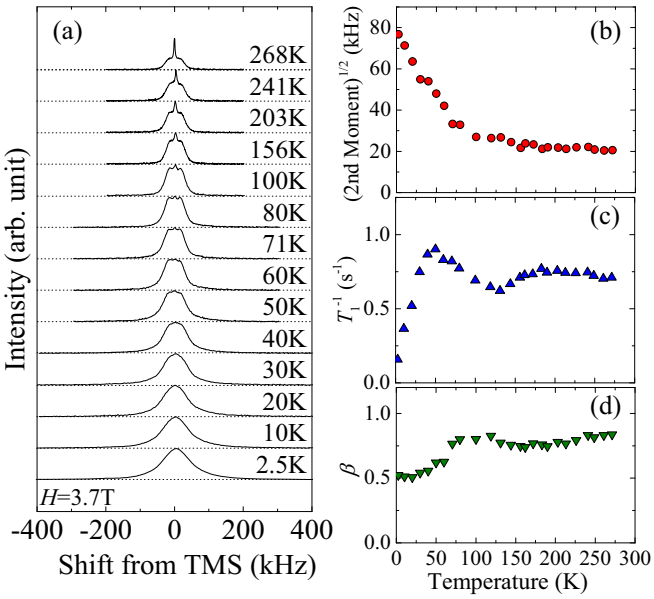

FIG. 2. (a) Temperature dependence of ^{1}H-NMR spectra for the polycrystalline $Pd(tmdt)_2$. (b)–(d) Temperature dependence of (b) the square root of the second moment, (c) the nuclear spin-lattice relaxation rate T_1^{-1}, and (d) the stretched exponent β.

measured under a magnetic field of 3.7 T for temperatures from 271 down to 2.5 K. The NMR spectra were obtained by the Fourier transformation of the so-called solid-echo signals following a $(\pi/2)_x$-$(\pi/2)_y$ pulse sequence, where x and y stand for the axes in the rotational frame [12]. The typical width of the $\pi/2$ pulse was 1.4 μs, which was much smaller than the inverse of the spectral width; hence, all of the nuclear spins are exhaustively driven into resonance. Below 100 K, where the spectra were progressively broadened upon cooling, we squeezed the pulse width down to 1.1 μs to cover the whole spectral frequency. The nuclear spin-lattice relaxation curves were obtained from the recovery of the echo intensity following saturation comb pulses.

The μSR experiments were conducted in the DOLLY area at the Paul Scherrer Institut (PSI) using a continuous muon beam with the spin polarization parallel to the beamline. The polycrystals weighing about 20 mg were wrapped in silver foil. Measurements were performed under zero magnetic field at temperatures from 150 K down to 2 K to cover the region of the magnetic transition.

III. RESULTS

Figure 2(a) shows the ^{1}H-NMR spectra at various temperatures. The spectral position is temperature-insensitive because the Knight shift is too small to be resolved, reflecting the small hyperfine coupling with the conduction electrons at the proton sites. The spectral width defined by the square root of the second moment, which measures the spectral width, is about 20 kHz at 271 K [Fig. 2(b)]. This value is explained reasonably by the nuclear dipole interaction between protons in the trimethylene group. Below 100 K, the spectra get broadened and spread over a frequency range of $\pm$200 kHz around the origin of shift at low temperatures. As shown in Fig. 2(b), the square root of the second moment starts to increase at 100 K and reaches a value of 77 kHz at the lowest temperature. This line broadening indicates the generation of local fields at the proton sites and provides microscopic evidence for a magnetic order. For powdered samples, any kind of magnetic order, whether ferromagnetic or antiferromagnetic, causes a broadening of the spectrum. In the case of ferromagnetic order, the isotropic term of a hyperfine field gives an additional one-sided shift of the broadened line; however, this is not the case shown in Fig. 2(a). Furthermore, spontaneous magnetization does not appear below the ordering temperature [10]. These experimental features indicate that $Pd(tmdt)_2$ undergoes an antiferromagnetic transition.

In what follows, we estimate the antiferromagnetic moment from the observed spectral width. According to the molecular-orbital calculations, the $p\pi$ orbital extends over the tmdt ligand, but the spin population on the proton sites is negligibly small. Therefore, we make a reasonable assumption that the local field at the proton sites is mainly generated by the dipole field of the $p\pi$ electron spin of $S = 1/2$ that is distributed in a tmdt ligand. Even in the presence of the isotropic hyperfine coupling between the electrons and protons, the antiferromagnetic moment should flop and be directed perpendicular to the applied field of 3.7 T, thus being unlikely to have a contribution to the line broadening. In the present analysis, we consider local fields at the proton sites from the $p\pi$ spins in ten neighboring molecules as well as in the on-site molecule. Because the antiferromagnetic spin structure is not known, we assumed seven possible antiferromagnetic spin arrangements, in which one or more out of three nearest-neighbor interactions are antiferromagnetic. Using the atomic parameters obtained by an x-ray diffraction study [10] and the atomic profile of the Mulliken population of the $p\pi$ orbitals in tmdt, we calculated the dipole fields at a given proton site from the on-site and neighboring $p\pi$

spins, and then summed them up to get the total local field at the proton site. In the present experiment using a fine polycrystalline sample, the direction of the external magnetic field against the crystal grains in the sample is random. In addition, the magnetic easy axis is unknown. Taking these facts into account, we set the moment direction arbitrarily, keeping the spin-flop configurations, in the calculations of the dipole fields at the proton sites produced by the local moment directed perpendicular to the external field due to the spin flop. Note that NMR line shift or broadening is contributed to only by the local-field component parallel to the external field, i.e., the component normal to the ordered moment in the spin-flopped state. We calculated the dipole fields at the six proton sites in a tmdt ligand for all directions of the ordered moments. Since the distance and direction from the nearest $p\pi$ spins depend on the proton sites, the local field is different from site to site. However, what we need for the estimation of the antiferromagnetic moment is the averaged value of the local fields, which is characterized by the second moment. After performing all these calculations, the square root of the second moment expected if the $S = 1/2$ spins are fully ordered yields 330–820 kHz. The observed second moment of $(77\ \text{kHz})^2$ at 2.5 K include both the antiferromagnetic broadening in question and the nuclear dipole broadening. Assuming that the high-temperature values of the second moment, represented by the room-temperature value, $(21\ \text{kHz})^2$, come from the latter, the former contribution yields $(74\ \text{kHz})^2$ [$=(77\ \text{kHz})^2$–$(21\text{kHz})^2$]. This value points to the local moment of 0.05–0.11μ_B per tmdt ligand. The value, much smaller than the classical moment of 1μ_B, indicates the spin contraction or inhomogeneity in spin density. We also estimated the antiferromagnetic moment from the maximum value in the local-field distribution, which corresponds to the spectral edge. The comparison of the observed edge value of 200 kHz at 2.5 K and the calculated edge values gives the local moments of 0.14–0.34μ_B per tmdt ligand, which is substantially different from the values obtained from the second moment. This discrepancy between the two estimates suggests that the moment size is distributed inhomogeneously in the sample.

Figure 2(c) shows the temperature dependence of the nuclear spin-lattice relaxation rate T_1^{-1}. The relaxation curves of nuclear magnetization, defined by $1 - M(t)/M(\infty)$ [$M(t)$ is the nuclear magnetization at a time t after its saturation], were not the single-exponential functions because of the existence of six crystallographically different proton sites with different local fields and the powder distribution of the angle between the sample direction and the applied magnetic field. Therefore, we defined T_1^{-1} by fitting the relaxation curves to the stretched-exponential functions, $\exp[-(t/T_1)^\beta]$. As seen in Fig. 2(c), the T_1^{-1} forms a moderate peak around 200 K and gradually increases below 130 K, followed by a broad peak at approximately 50 K. The peak formation around 200 K is not of electronic origin but a molecular motional contribution, which has been observed in the isostructural M = Ni and Pt compounds [4]. The peak at 50 K is not explained by the molecular motion. The spectral broadening considered, the increase of T_1^{-1} below 130 K reflects the critical slowing down and/or the formation of inhomogeneous magnetic order. The broadness of the peak in T_1^{-1} suggests

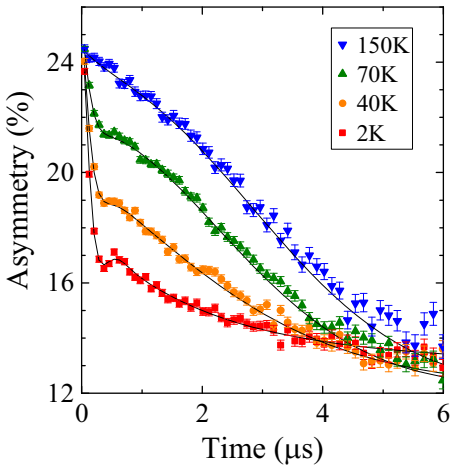

FIG. 3. Temperature dependence of the muon relaxation spectra for the polycrystalline $Pd(tmdt)_2$. Solid curves are the fitting functions of Eqs. (1) ($T > 100$ K) and (2) ($T < 90$ K).

that the ordering temperature is distributed over a wide range up to 130 K with a majority around 50 K. A gradual increase in NMR linewidth upon cooling as shown in Fig. 2(b) is a typical behavior of the inhomogeneous magnetic order with distributed ordering temperatures. In such a case, the sum of peaks in T_1^{-1} formed at each ordering temperature leads to a broadened peak around the temperature, where the weight of the distribution is maximum. The fitting exponent β, which measures the spatial distribution of T_1, is shown in Fig. 2(d). The value of β is almost constant ($\sim$0.8) for a wide temperature range above 70 K, but it decreases below 70 K, which signifies that a sizable fraction of the sample becomes magnetically ordered below this temperature.

To characterize the inhomogeneity of the antiferromagnetic order in $Pd(tmdt)_2$, we carried out the muon-spin resonance measurements. Figure 3 shows the forward-backward asymmetry of the detected positron emission following muon decay under a zero magnetic field. This asymmetry directly measures the time dependence of the implanted muon spin polarization under the influence of the local field at the muon site. The relaxation becomes faster at lower temperatures, and the shape of the relaxation function changes with temperature. At 2 K, the fast oscillation, i.e., the muon-spin precession signal, is clearly observed, which confirms the appearance of the antiferromagnetic ordering.

The asymmetry data for temperatures above 100 K were fitted with the function

$$A(t) = A_1 e^{-(\lambda_1 t)^\alpha} + A_2 e^{-\lambda_2 t} + A_{\text{bg}}, \quad (1)$$

where the first and second terms on the right side represent the slow and fast depolarizing components, respectively, and the third term expresses the background level. Below 90 K, the data were found to be well fitted by the form

$$A(t) = A_1 e^{-(\lambda_1 t)^\alpha} + A_3 \cos(\gamma_\mu H_{\text{int}} t + \phi) e^{-\lambda_3 t} + A_{\text{bg}}, \quad (2)$$

where the second term on the right side shows the muon-spin precession component. The parameters A_i and λ_i (i = –3)1 in Eqs. (1) and (2) are the initial asymmetries at $t = 0$ and the relaxation rates of each components, respectively. The exponent α is a variable shape parameter, which is 2 for the

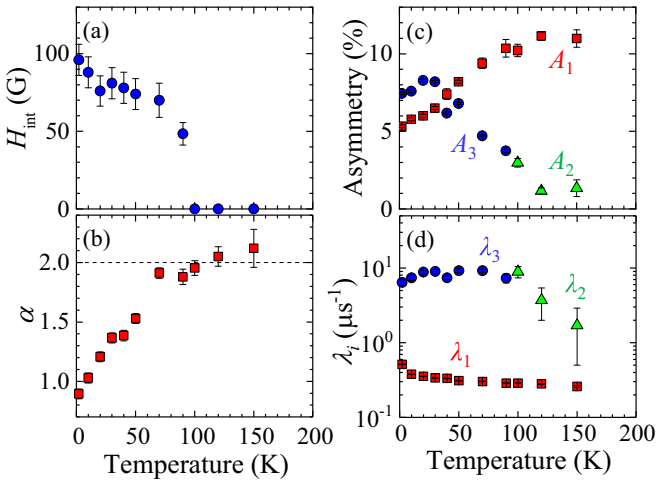

FIG. 4. Temperature dependences of (a) the internal magnetic field at muon sites, (b) the shape parameter of the slow depolarizing component, (c) the initial asymmetries, and (d) the relaxation rate. Red square, green triangle, and blue circle in (c) and (d) indicate the slow depolarizing component (A_1,λ_1), the fast depolarizing component (A_2,λ_2), and the precession component (A_3,λ_3), respectively.

Gaussian limit and 1 for the Lorentzian limit. The parameters γ_μ, $H_{\rm int}$, and ϕ are the muon gyromagnetic ratio, the internal magnetic field at muon sites, and the phase of the muon-spin precession, respectively. The fits of the above functions to the data are shown by solid lines in Fig. 3.

At 100 K, the local field $H_{\rm int}$ shows an abrupt increase [Fig. 4(a)], and the value of α [Fig. 4(b)] starts to deviate from 2 and decreases toward 1 upon cooling. The Gaussian relaxation functions in the higher-temperature range are regarded as resulting from the nuclear-dipole fields. At lower temperatures, the relaxation function approaches the Lorentzian form, suggesting some contribution to the relaxation due to electronic spin fluctuations. The amplitude of this slow depolarizing signal, A_1, remains even at the lowest temperature, coexisting with that of the muon-spin precession signal, A_3 [Fig. 4(c)]. The volume ratio of the antiferromagnetic phase is about 60% of the total. The impurity-spin concentration determined from the Curie contribution to the magnetic susceptibility is 0.8% [10], which cannot explain the nonoscillating component. This indicates the phase separation or admixture within the sample, i.e., some remnant volume of the paramagnetic or nonmagnetic state exists in the host of the antiferromagnetic ordered state. Since the moment size is found distributed inhomogeneously, the nonoscillating component may contain the ordered state with a relatively small moment. We note that even nonordered domains show more strongly enhanced spin fluctuations than in the high-temperature paramagnetic state above 100 K, as evidenced by the α values [Fig. 4(b)]. The relaxation rate λ_i measures the local field distribution. λ_1 is gradually increased with lowering temperature below about 50 K [Fig. 4(d)], which, in conjunction with the gradual change from $\alpha = 2$ to 1, suggests the development of short-range spin correlation in the nonordered domains. Assuming the static contribution, the measured $\lambda_3 = 6.4$–9.2 μs^{-1} corresponds to the distribution width of 75–110 G, which is comparable to the value of $H_{\rm int}$.

To evaluate the size of the ordered moment, we performed an electrostatic potential calculation to determine the stable muon position in $Pd(tmdt)_2$. The muon state was calculated using a computational code QMAS in a similar approach to obtaining the positron state [13]. In the Kohn-Sham-like equation, the muon mass was used instead of the positron one. Note that we neglected the muon effect on the electronic structure and the atomic arrangement, which is reasonable since we consider a delocalized muon state. The obtained center of muon distribution is shown in Figs. 1(b) and 1(c). We calculated the magnetic dipole field for the muon site in the same way as described in the analysis of the NMR results. Comparing the dipole field with the experimentally obtained $H_{\rm int}$ value, we estimated the ordered moment size at 0.08–0.12μ_B per tmdt ligand. This value agrees well with that obtained from the analysis of the ^{1}H-NMR spectra, which suggests that our muon-site estimation and the evaluated moment are reasonable.

IV. DISCUSSIONS

Our NMR and μSR results confirmed the antiferromagnetic order in $Pd(tmdt)_2$. Regarding the origin of the antiferromagnetic order, two cases are conceivable. One is the formation of a spin-density wave due to nesting of the Fermi surfaces. According to the electronic band-structure calculations, however, $Pd(tmdt)_2$ has semimetallic Fermi surfaces, which have no preferential vectors for nesting [10]. The other case is the exchange interaction in an antiferromagnetic Mott insulator. Since appreciable antiferromagnetic fluctuations are observed in the metallic Ni and Pt compounds [8], strong exchange interactions among $p\pi$ electrons are likely present in the Pd compound as well. In this context, the semiconducting resistivity behavior of $Pd(tmdt)_2$ is understandable as an indication of the Mott insulating state. However, its activation energy is only 3–9 meV, and the absolute value of resistivity is as low as 0.01 Ω cm around room temperature [10]. It is theoretically suggested that the impurity effect is significant for correlated electrons situated close to the Mott transition [14,15]. Indeed, it is reported that disorder introduced by x-ray irradiation to a marginal Mott insulator, κ-$(ET)_2Cu[N(CN)_2]Cl$ [16], strongly affects both charge and spin degrees of freedom; that is, the irradiation diminishes the charge gap [17] and suppresses the antiferromagnetic order [18]. Therefore, the marginal insulating behavior and the depressed inhomogeneous magnetic moments of $\sim 0.1\mu_B$ revealed here are compatible with the view that $Pd(tmdt)_2$ is a disordered marginal Mott insulator with an antiferromagnetic order driven by exchange interactions. The disorder in the present sample can be caused by the paramagnetic impurities of 0.8%, which was determined from the Curie contribution to the magnetic susceptibility [10]. This impurity concentration is, however, comparable to those of $Pt(tmdt)_2$ (0.6%) and $Ni(tmdt)_2$ (0.8%) [4]. It is likely that the disorder effect is enhanced particularly in $Pd(tmdt)_2$ due to the proximity to the Mott transition.

The Mott insulating state of the $p\pi$ electrons was found in the isostructural compound $Cu(tmdt)_2$ with $p\pi$-$dp\sigma$ multiorbital bands, while its ground state is a spin-gapped state in contrast to the present case [5]. The network of inter-tmdt

transfer integrals is quasi-two-dimensional and reduced to an anisotropic dimerized square lattice [5], as shown in Fig. 1(d). According to the theoretical studies based on the two-dimensional Heisenberg model on such an anisotropic dimerized square lattice, the magnetic ground state is determined by the values of α/J and J'/J, where J and α are the intrachain alternating exchange interactions ($J > \alpha$), and J' is the interchain exchange interaction [19]. Although the transfer integrals (t) in $Pd(tmdt)_2$ are unknown, the isostructural $Ni(tmdt)_2$ and $Cu(tmdt)_2$ commonly possess the largest transfer integral between tmdt's along the [111] direction (t_B) and the second and third largest ones along the [001] and [100] directions (t_Q and t_A), respectively [Figs. 1(b) and 1(c)]. According to the x-ray diffraction study [10], the lattice parameters of $Pd(tmdt)_2$ are in between those of $Ni(tmdt)_2$ and $Cu(tmdt)_2$, and the values of the intermolecular nearest S-S distances along the [111], [001], and [100] directions in $Pd(tmdt)_2$ are rather close to those in $Ni(tmdt)_2$ than in $Cu(tmdt)_2$; thus, the values of α/J and J'/J for $Ni(tmdt)_2$ can be references for $Pd(tmdt)_2$. The exchange interaction is proportional to t^2, which yields $(\alpha/J, J'/J, J'/\alpha) = (t_Q^2/t_B^2, t_A^2/t_B^2, t_A^2/t_Q^2) = (0.35, 0.15, 0.43)$ for $Pd(tmdt)_2$, and $(0.29, 0.13, 0.45)$ for $Cu(tmdt)_2$ [20]. For $J'/\alpha = 0.45$, the theoretical simulations give the critical values of $(\alpha_c/J, J_c'/J) \sim (0.71, 0.32)$, below which the ground state is a spin-gapped dimer state [19]. Therefore, the antiferromagnetic state in $Pd(tmdt)_2$ is not understood in the framework of the Heisenberg model.

A conceivable reason for the discrepancy is that the Heisenberg model does not provide an appropriate description for the present system, which is considered to be located near the Mott transition boundary because of the weak semiconducting behavior of resistivity [10]. In the vicinity of the Mott transition, the interactions among electron spins can be complicated by the involvement of next-nearest and ring exchange interactions beyond the simple Heisenberg model. Another ingredient to be taken into account is disorder, which is known to induce long-ranged staggered moments in low-dimensional spin-gapped states [21–24]. According to a theoretical study [24], impurity doping, or site dilution, can induce an antiferromagnetic long-range order in dimerized Heisenberg spins on an anisotropic square lattice, which are otherwise spin-gapped. The indication of the coexisting antiferromagnetic and paramagnetic/nonmagnetic phases in $Pd(tmdt)_2$ is not incompatible with this scenario.

In conclusion, the present NMR and μSR experiments have revealed that the single-component molecular material $Pd(tmdt)_2$ is an antiferromagnet with small and distributed moments of the order of $0.1\mu_B$ but with the magnetic ordering onset exceeding 100 K. The gossamer nature of the moment profile is explainable in terms of the proximity to the Mott transition boundary and the effect of disorder. The present results provide an example of an antiferromagnetic order in purely $p\pi$ electronic systems, which sets in at as high as 100 K even without hybridization of the $dp\sigma$ electrons. This finding provides insight into the interplay of the two orbitals in the diverse electronic states emerging in $M(tmdt)_2$, which include a $p\pi$ correlated metal (M = Ni and Pt) [4], a $p\pi$ spin-gapped Mott insulator (M = Zn) [6], a hybrid Mott insulator with a $p\pi$ spin singlet and a $dp\sigma$ antiferromagnet (M = Cu) [5], and a $p\pi$-$dp\sigma$ hybrid antiferromagnetic metal (M = Au) [20,25].

ACKNOWLEDGMENTS

The authors thank P. Biswas for experimental support. This work was supported by the JSPS Grants-in-Aid for Scientific Research (S) (Grant No. 25220709) and for Scientific Research (C) (Grants No. 17K05846 and No. 17K05532).

[1] H. Tanaka, Y. Okano, H. Kobayashi, W. Suzuki, and A. Kobayashi, Science **291**, 285 (2001).
[2] A. Kobayashi, E. Fujiwara, and H. Kobayashi, Chem. Rev. **104**, 5243 (2004).
[3] A. Kobayashi, Y. Okano, and H. Kobayashi, J. Phys. Soc. Jpn. **75**, 051002 (2006).
[4] R. Takagi, K. Miyagawa, M. Yoshimura, H. Gangi, K. Kanoda, B. Zhou, Y. Idobata, and A. Kobayashi, Phys. Rev. B **93**, 024403 (2016).
[5] R. Takagi, T. Hamai, H. Gangi, K. Miyagawa, B. Zhou, A. Kobayashi, and K. Kanoda, Phys. Rev. B **95**, 094420 (2017).
[6] R. Takagi, H. Gangi, K. Miyagawa, B. Zhou, A. Kobayashi, and K. Kanoda, Phys. Rev. B **95**, 224427 (2017).
[7] S. Ishibashi, K. Terakura, and A. Kobayashi, J. Phys. Soc. Jpn. **77**, 024702 (2008); **83**, 068003 (2014).
[8] C. Rovira, J. J. Novoa, J. L. Mozos, P. Ordejon, and E. Canadell, Phys. Rev. B **65**, 081104(R) (2002).
[9] B. Zhou, A. Kobayashi, Y. Okano, T. Nakashima, S. Aoyagi, E. Nishibori, M. Sakata, M. Tokumoto, and H. Kobayashi, Adv. Mater. **21**, 3596 (2009).
[10] S. Ogura, Y. Idobata, B. Zhou, A. Kobayashi, R. Takagi, K. Miyagawa, K. Kanoda, H. Kasai, E. Nishibori, C. Satoko, and B. Delley, Inorg. Chem. **55**, 7709 (2016).
[11] H. Tanaka, M. Tokumoto, S. Ishibashi, D. Graf, E. S. Choi, J. S. Brooks, S. Yasuzuka, Y. Okano, H. Kobayashi, and A. Kobayashi, J. Am. Chem. Soc. **126**, 10518 (2004).
[12] C. P. Slichter, *Principles of Magnetic Resonance* (Springer, Heidelberg, 1998).
[13] S. Ishibashi, J. Phys. Soc. Jpn. **84**, 083703 (2015).
[14] H. Shinaoka and M. Imada, Phys. Rev. Lett. **102**, 016404 (2009).
[15] H. Shinaoka and M. Imada, J. Phys. Soc. Jpn. **78**, 094708 (2009).
[16] K. Kanoda, Hyperfine Interact. **104**, 235 (1997); J. Phys. Soc. Jpn. **75**, 051007 (2006).
[17] T. Sasaki, Crystals **2**, 374 (2012).
[18] T. Furukawa, K. Miyagawa, T. Itou, M. Ito, H. Taniguchi, M. Saito, S. Iguchi, T. Sasaki, and K. Kanoda, Phys. Rev. Lett. **115**, 077001 (2015).
[19] M. Matsumoto, C. Yasuda, S. Todo, and H. Takayama, Phys. Rev. B **65**, 014407 (2001).
[20] H. Seo, S. Ishibashi, Y. Otsuka, H. Fukuyama, and K. Terakura, J. Phys. Soc. Jpn. **82**, 054711 (2013).
[21] E. F. Shender and S. A. Kivelson, Phys. Rev. Lett. **66**, 2384 (1991).

[22] H. Fukuyama, T. Tanimoto, and M. Saito, J. Phys. Soc. Jpn. **65**, 1182 (1996).

[23] M. C. Martin, M. Hase, K. Hirota, G. Shirane, Y. Sasago, N. Koide, and K. Uchinokura, Phys. Rev. B **56**, 3173 (1997).

[24] C. Yasuda, S. Todo, M. Matsumoto, and H. Takayama, Phys. Rev. B **64**, 092405 (2001).

[25] Y. Hara, K. Miyagawa, K. Kanoda, M. Shimamura, B. Zhou, A. Kobayashi, and H. Kobayashi, J. Phys. Soc. Jpn. **77**, 053706 (2008).